THE ASTROPHYSICAL JOURNAL SUPPLEMENT SERIES, 127:339–346, 2000 April

NUMERICAL SIMULATIONS OF DEEP NONLINEAR RICHTYMER-MESHKOV INSTABILITY

MARY JANE GRAHAM
Department of Mathematical Sciences, United States Military Academy, West Point, NY 10996-1786, and Army Research Laboratory, Aberdeen Proving Ground, MD 21005-5066

AND

QIANG ZHANG
Department of Mathematics, City University of Hong Kong, 83 Tat Chee Avenue, Kowloon, Hong Kong, and Department of Applied Mathematics and Statistics, State University of New York at Stony Brook, Stony Brook, NY 11794-3600
Received 1999 January 19; accepted 1999 August 3

ABSTRACT

The Richtmyer-Meshkov (RM) instability is an interfacial instability between two fluids of different densities driven by shock waves and plays an important role in the studies of inertial confinement fusion and supernova. So far, most of the studies are for RM unstable interfaces driven by weak or intermediate shocks in planar geometry. Some results are given for the weak shock case in cylindrical geometry. For experiments conducted at Nova laser, the unstable material interface is accelerated by very strong shocks. We also present scaling laws for the RM unstable interface driven by strong imploding and exploding shocks.

Subject headings: hydrodynamics — instabilities — method: laboratory — shock waves

1. INTRODUCTION

The instability of a material interface under an acceleration of an incident shock was predicted theoretically by Richtmyer in 1960 (Richtmyer 1960). Ten years later, Meshkov confirmed, experimentally, Richtmyer's prediction (Meshkov 1970). Since then, this interfacial instability is known as the Richtmyer-Meshkov (RM) instability. In the first part of this paper, some results are presented for the weak shock case (for more detailed results, see Zhang & Graham 1998). We consider the perturbed circular material interface driven by a circular shock wave for the single mode RM instability in cylindrical geometry.

In plane geometry, there are two classes of RM unstable systems: a shock wave collides with the material interface from the light fluid phase to the heavy fluid phase, and vice versa. In curved geometry, there are four classes. The first class is a shock wave exploding from light fluid to heavy fluid (light-exploding-heavy). The second class is a shock wave imploding from light fluid to heavy fluid (light-imploding-heavy). The second class is a shock wave imploding from light fluid to heavy fluid (light-imploding-heavy). The third class is a shock wave exploding from heavy fluid to light fluid (heavy-exploding-light). The fourth class is a shock wave imploding from heavy fluid to light fluid (heavy-imploding-light). These four classes are sketched in Figures 1*a*–1*d*, respectively. This classification can also be used for the RM instability in spherical geometry. In Figure 1, as well as in other figures, only the results in the first quadrant are shown. The general features of the development of the RM interface in cylindrical geometry are the following. When an incident shock collides with the material interface, it bifurcates into a transmitted shock and a reflected wave. This is the bifurcation stage, or the shock-contact interaction stage. At the end of the interaction stage, both the transmitted shock and the reflected wave detach from the material interface. One wave propagates away from the center (or origin), and for an open space, the outgoing wave will not interact with the material interface again. The other wave propagates toward the center (or origin). Accelerated by incident shock, the material interface becomes unstable and fingers grow to form bubbles and spikes. Later, the wave that moved toward the center reflects back from the origin. As the reflected wave propagates from the origin, it collides with the material interface again, which is known as reshock. A second bifurcation occurs. Thus, the occurrence of reshock is unavoidable in curved geometry. In Figure 2, the features for a system in class 3 (heavy-exploding-light) are demonstrated. The initial material interface is sinusoidal. Figure 2*a* is the initial configuration. Figure 2*b* is the refraction process (bifurcation stage). The incident shock wave has collided with the material interface and immediately bifurcates into a transmitted shock wave and a reflected wave. For class 3, the reflected wave is a rarefaction. It is important to note that the shock-contact collision will cause the initial perturbation amplitude, a, to decrease. In Figure 2*c* the wave bifurcation process is over, all the waves have detached from the material interface. A reflected rarefaction wave propagates toward the origin, and a transmitted shock propagates outward. Note that for Figure 2*a*–2*c*, the region shown is an enlarged version. In Figure 2*d* the system develops into the nonlinear fingers shown. The curve labeled RTE is the trailing edge of the reflected rarefaction wave. The heavy fluid has deeply penetrated the light fluid forming spikes. The light fluid has surrounded the heavy fluid forming bubbles. The flattened mushroom capped spike and the secondary shoulders on the fingers have been produced by the effects of the Kelvin-Helmholtz instability at the tips and the shoulders. A comparison of the shape of the material interface in Figure 2*c* with the initial interface shape given in Figure 2*a*, shows that the fingers are inverted. This phenomenon is known as phase inversion and is expected when a shock collides with a material interface from a heavy fluid phase to a light fluid phase (Yang et al. 1994).

The general features of the RM unstable system in the first, the second and the fourth classes are similar to the one shown in Figure 2. When the incident shock travels from a

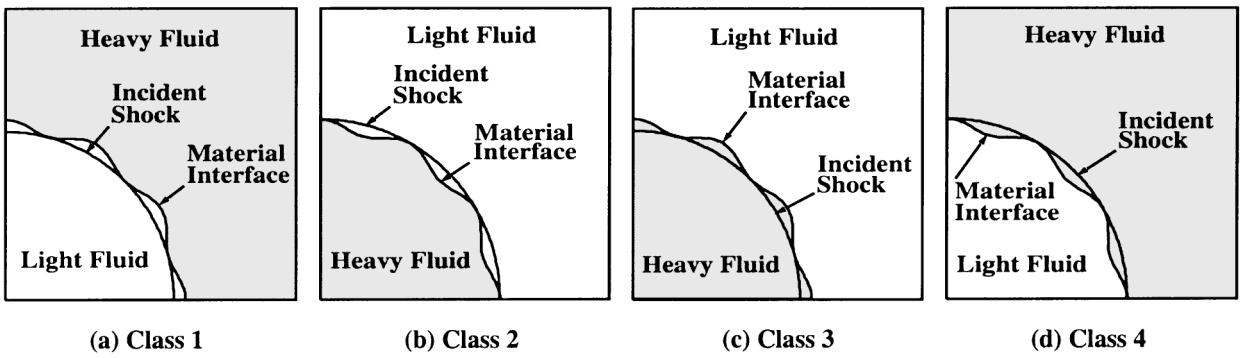

FIG. 1.—A classification of RM unstable systems in curved geometry. (*a*) Class 1: an incident shock propagates outward from a light fluid toward a heavy fluid, (light-exploding-heavy). (*b*) Class 2: an incident shock propagates inward from a light fluid toward a heavy fluid, (light-imploding-heavy). (*c*) Class 3: an incident shock propagates outward from a heavy fluid toward a light fluid, (heavy-exploding-light). (*b*) Class 4: an incident shock propagates inward from a heavy fluid toward a light fluid (heavy-imploding-light).

light fluid to a heavy fluid (class 1 and class 2), the reflected wave is a shock wave; and the phenomenon of phase inversion does not occur unless the shock is very strong.

The method of front tracking (Chern et al. 1986) has been used in our numerical simulations. Front tracking is an adaptive computational method where a low-dimensional, moving grid is embedded in a high-dimensional fixed grid. The low-dimensional, moving grid is fitted to and moves dynamically with, the discontinuity fronts in the flow, such as the material interface, where the density is discontinuous,

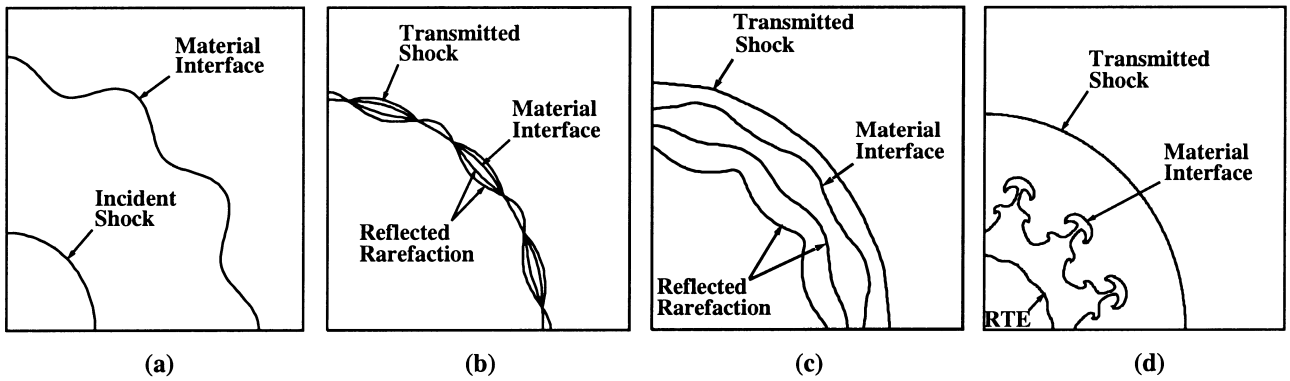

FIG. 2.—A schematic showing the general features of the RM instability in cylindrical geometry. The heavier gas is located behind the contact discontinuity. Part (*a*), (*b*), and (*c*) have been enlarged. (*a*) initial conditions; (*b*) refraction process; (*c*) reflected rarefaction moving radially toward origin, transmitted shock moving radially outward, deflected contact (phase inverted); (*d*) nonlinear finger growth, spikes of heavy fluid penetrate lighter fluid, bubbles of light fluid surround heavy fluid.

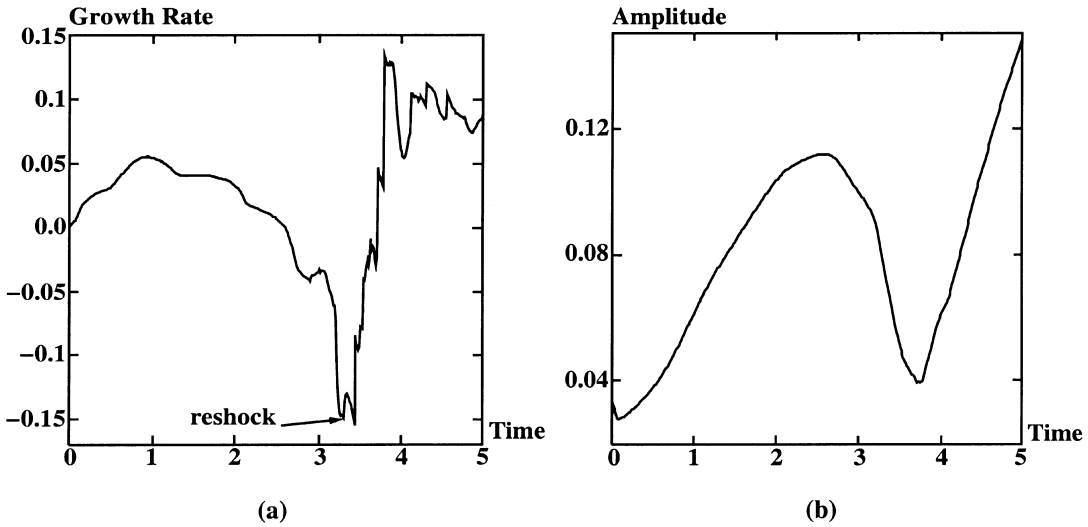

FIG. 3.—Data for class 2 (light-imploding-heavy). A shock of Mach number 1.2 implodes from air to SF_6. Figure contains reshock at $\tilde{t} = 3.25$, phase inversion between $\tilde{t} = 3.25$ and $\tilde{t} = 4.1$, and after phase inversion growth rate. (*a*) Perturbation growth rate $\dot{a}(t)$ vs. time. (*b*) Perturbation amplitude $a(t)$ vs. time.

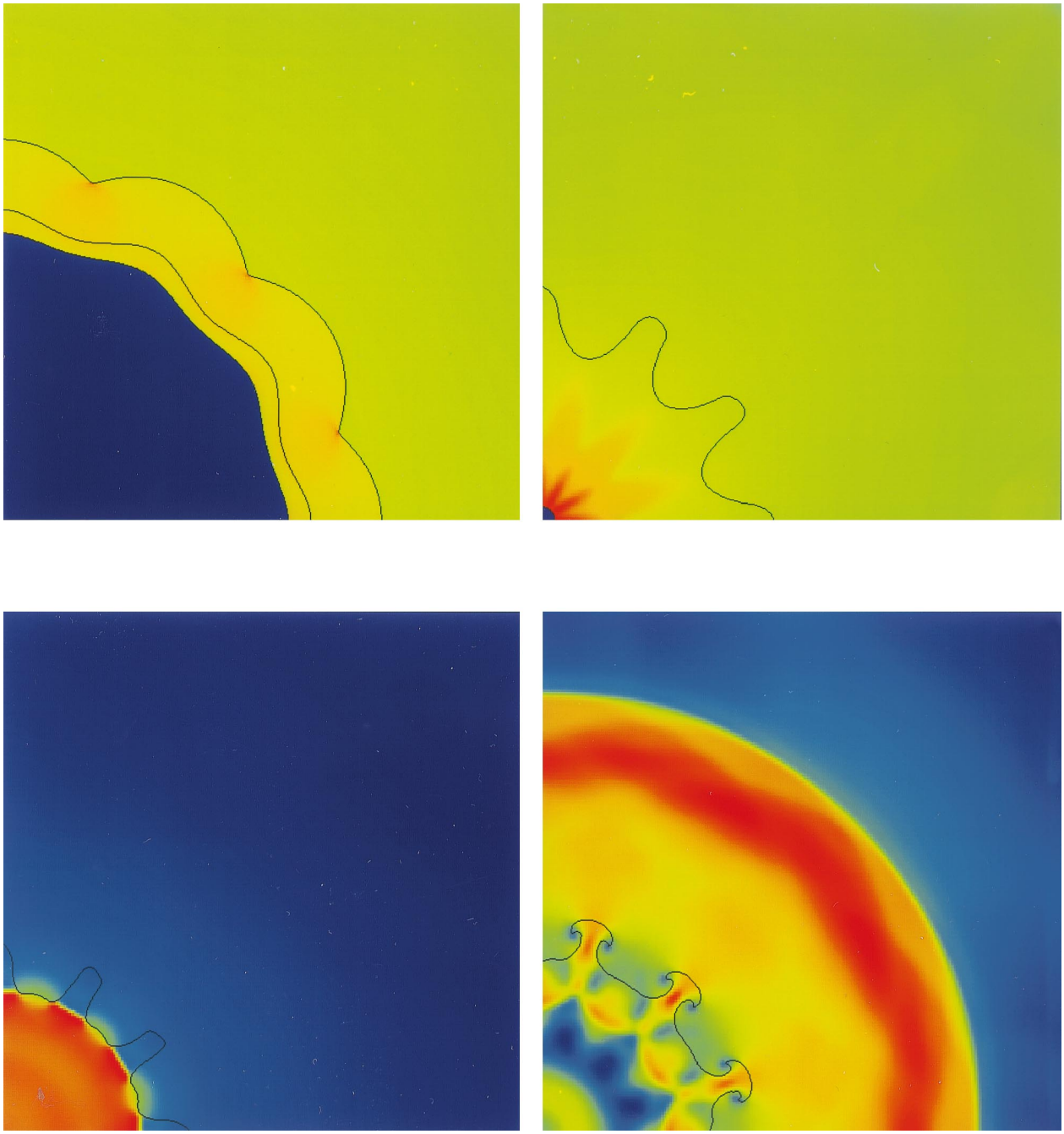

FIG. 4.—Evolution of material interface for class 2 at $\tilde{t} = 0.27$, 2.0, 3.9, and 4.2. The figure shows: (*upper left*) interface after bifurcation, reflected shock (RS) moves radially inward, transmitted shock (TS) moves radially outward; (*upper right*) RS exited computational domain, TS about to enter origin; (*lower left*) TS bounced back from origin and reshocked the material interface, causing phase inversion; and (*lower right*) nonlinear finger growth at late time, with completed phase inversion.

or the shock interface, where the pressure is discontinuous. In these studies, a front can also be the leading or trailing edges of a rarefaction wave. The front tracking method uses the exact mathematical property, known as the Riemann problem solution, to advance the position of the discontinuity interface and to update the physical quantities on each side of the interface. See Chern et al. (1986) for further details of the front tracking method and its implementation.

2. THE NONLINEAR GROWTH RATES

The growth rate of the fingers at a RM unstable material interface in the nonlinear regime is one of the most important physical quantities. In this section, we present the results from the numerical study of this growth rate for class 2 (light-imploding-heavy). The qualitative understanding in this section is applicable to fingers in spherical geometry as well. The numerical results from four different classes can be found in Zhang & Graham (1998).

The reflected wave is a shock unless the incident shock is very strong. We study the growth rate, the amplitude, and the shape of the material interface. There is a significant phenomena that occurs for class 2 at the time of reshock. In the imploding case, the initial incident shock wave travels from a light fluid into a heavy fluid. After bifurcation the transmitted shock is traveling through a heavy fluid. It bounces back from the origin through this heavy fluid

toward a light fluid as in class 3; therefore, at reshock there is a phase inversion. Figure 3 shows the growth rate versus time and the perturbation amplitude versus time. A weak shock of Mach number 1.2 travels from air to SF_6. There are $n = 12$ fingers for the full (circular) domain. The initial position of the material interface is located at the dimensionless radius of 1, and the initial perturbation amplitude is 0.033. The evolution of the interface is shown at four times during the simulation in Figure 4.

The initial configuration can be seen in Figure 1*b*. The upper left frame of Figure 4 shown herein is after the incident shock has refracted through the material interface and corresponds to $\tilde{t} = 0.27$. The transmitted shock travels radially in toward the origin (or center), and the reflected shock moves radially outward. Note the secondary waves behind the reflected shock. Again at a much earlier time when the transmitted shock and the reflected shock were closer to the material interface, the secondary waves behind them impinged on the material interface causing the first slight dip in the growth rate graph at $\tilde{t} = 0.5$. The implosion of the incident shock causes the material interface to move toward the origin at the early stage of the development of the finger growth and continues to do so until the transmitted shock has bounced back from the origin. This can be seen in the upper right frame of Figure 4 ($\tilde{t} = 2.0$). By $\tilde{t} = 2.0$, the reflected shock has exited the computational domain, and the transmitted shock is about to converge at the origin. Since the wavelength decreases as the material interface moves inward, the growth rate in the imploding case is higher than that in the plane geometry. This can be easily understood from the fact that the linear growth rate in plane geometry is inversely proportional to the wave length. As the material interface moves closer to the origin, the velocity decreases. The slow down of the velocity field causes the slow down of the growth of the fingers at intermediate times ($1.6 \leq \tilde{t} \leq 2.85$).

Before the time of reshock, the bounced shock is propagating from a heavy fluid to a light fluid and will cause a phase inversion of the material interface upon reshock. The reshock can be seen in the growth rate graph as the steep vertical jump down at $\tilde{t} = 3.25$ and the kink in the amplitude graph at the same time.

The bottom left frame of Figure 4 shows the interface a short time after reshock, when the bifurcation process is taking place. It can be seen that the transmitted shock is nestled between the peaks, and the reflected rarefaction

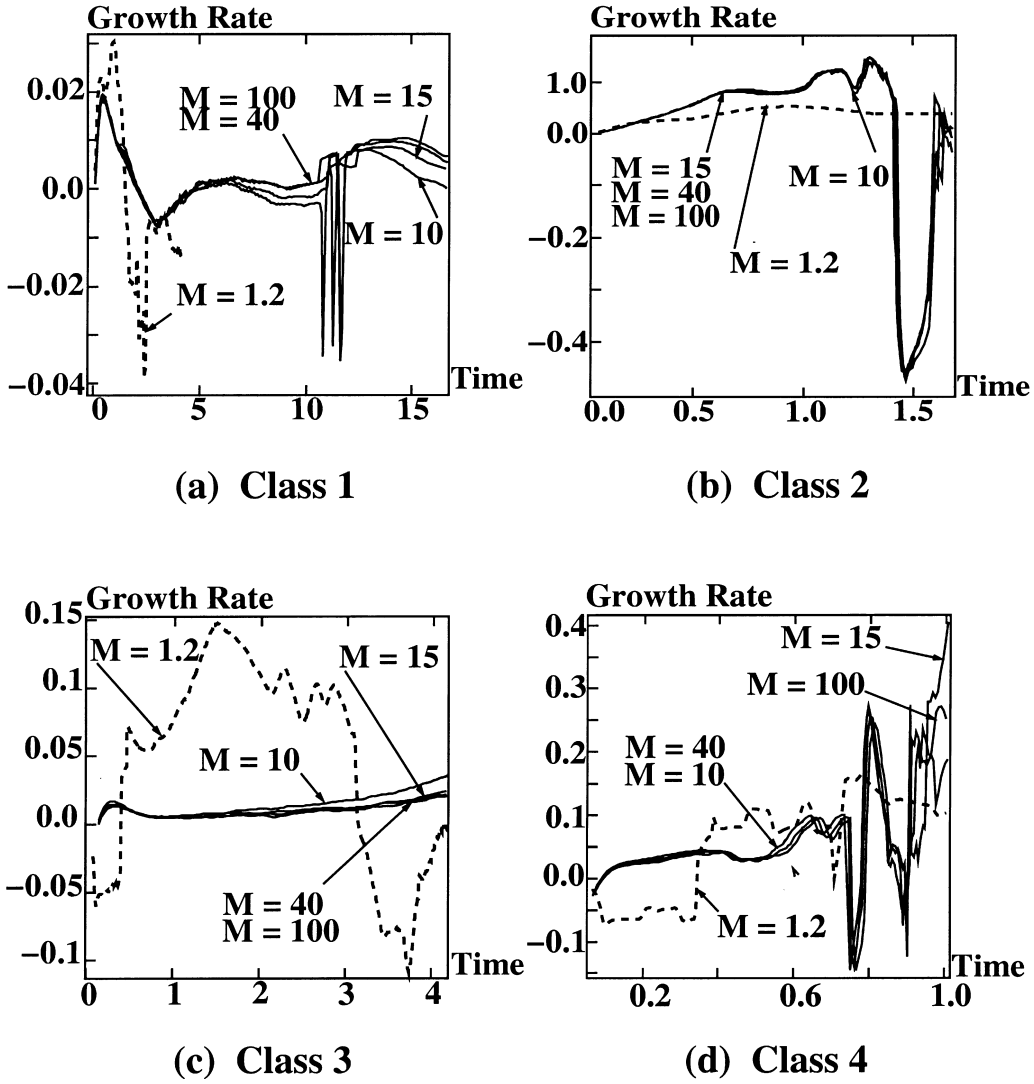

FIG. 5.—Comparsion of the scales perturbation growth rate vs. scaled time for various Mach numbers—namely, $M = 1.2$, 10, 15, 40, and 100. The dashed curves are for $M = 1.2$. The shocked Atwood number of the air_6 interface is $A = 0.67213$.

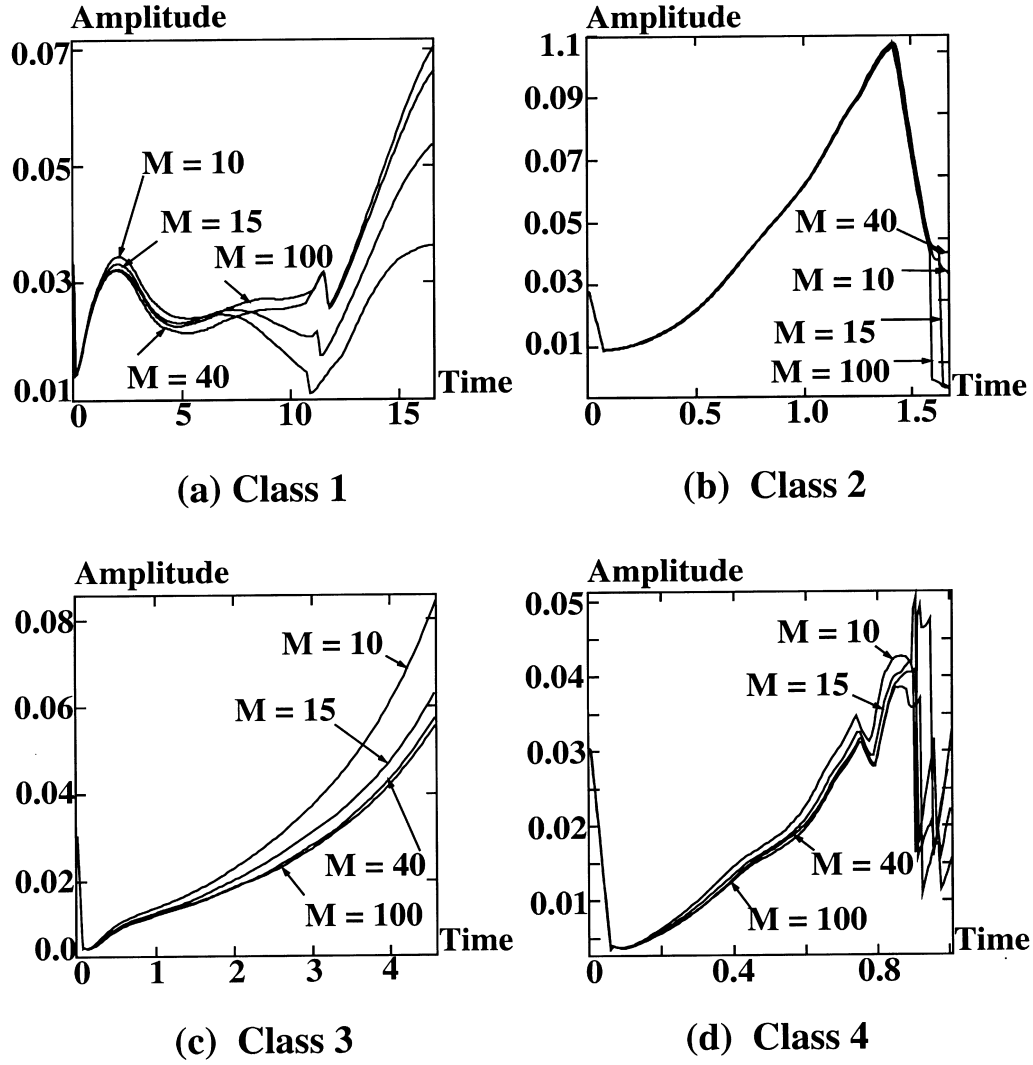

FIG. 6.—Comparison of the perturbation amplitude vs. time for various Mach numbers, namely, $M = 10, 15, 40$, and 100

is forming and beginning to move toward the origin. The reflected wave is a rarefaction in this case since the bounced shock was traveling through a heavy fluid to a light fluid.

Again, the reshock in this case causes a phase inversion: namely, the portion of fluid in one region which appears in the figure as valleys (and are bubbles of light fluid) and the other portion of fluid which appears in the figure as peaks (and are spikes of heavy fluid) prior to reshock will start to change positions after reshock and shock refraction. That is to say, the valleys (bubbles) will become peaks (spikes) and the peaks (spikes) will become valleys (bubbles). The process of phase inversion due to reshock is demonstrated in the bottom two frames of Figure 4. Note the effects of the Kelvin-Helmholtz instability (shearing effects) acting on the spikes, forming the beginning of the familiar mushroom roll-ups (*bottom right panel*). The phase inversion process can be seen in the growth rate (Fig. 3*a*) taking place from the time of reshock at $\tilde{t} = 3.25$ and continuing until approximately $\tilde{t} = 4.1$. It can be seen in the amplitude graph at $\tilde{t} = 3.75$.

Secondary shocks also form in this simulation and propagate radially outward. They reshock the material interface before the main reshock caused by the wave bounced back from the origin. This is seen in the slight bump on Figure 3*a* in the time interval $2.85 < \tilde{t} < 3.1$, which is just before the reshock.

Finally, at a much later time, the nonlinear finger growth has formed into the full bubbles of light fluid and spikes of heavy fluid with the caps at the fingers as previously described, and the phase inversion is completed (see the bottom right frame of Fig. 4). One can also see the second transmitted shock, this time moving away from the origin. There is a significant amount of wave interaction inside the region between the reshocked material interface and the reflected rarefaction. The highly nonlinear activity there accounts for the series of reshocks (or oscillations) seen in Figure 3*a* at $\tilde{t} > 4.18$.

3. STRONG SHOCKS

The study of Richtmyer-Meshkov instabilities has attracted many researchers in recent years, due to the fact that this instability plays an important role in inertial confinement fusion and supernova. Experimental studies of the RM unstable interface driven by strong shocks (Mach > 20) have been achieved (Dimonte, Frerking, & Schneider 1996). With the rapid advances in computing technology, direct numerical simulation has become popular. It provides us with a new way to study RM unstable systems.

Most of the numerical studies of the RM unstable system have been and are being performed in planar geometry and for incident shocks with small or intermediate Mach number. At this time, we consider the RM unstable interface driven by strong shocks in cylindrical geometry and establish an important scaling law. This scaling law will allow researchers to significantly reduce the number of experiments and numerical simulations required in the study of RM unstable interfaces driven by strong shocks.

How will the incident shock strength affect the development of RM instability? In general, the stronger the incident shock is, the faster the material interface will be accelerated and the faster the transmitted shock and reflected rarefaction wave travel. The phenomena of reshock will occur at an earlier time for systems accelerated by strong shocks. Therefore, dimensional units are not appropriate for studying the scaling behavior of RM unstable system driven by strong shocks. In order to reveal the scaling behavior of RM unstable systems, we introduce the following scaled dimensionless quantities:

$$\tilde{r} = \frac{r}{R_0}, \quad \tilde{v} = \frac{v}{W_i}, \quad \tilde{t} = \frac{W_i t}{R_0}.$$

Here R_0 is the mean radius of the initial material interface at $t = 0$, and W_i is the speed of the incident shock. In these scaled dimensionless units, the initial location of the material interface is given by $\tilde{r} = 1 + \tilde{a}_0 \cos(m\phi)$. Here $\tilde{a}_0 = a_0/R_0$ is a dimensionless perturbation amplitude, and a_0 is a dimensional perturbation amplitude.

The size of the mixing zone between the light and heavy fluids, i.e., the radial distance of the peaks and valleys along the material interface is a very important quantity for the RM unstable system. We define the overall growth rate and the amplitude of the RM unstable interface in cylindrical geometry as

$$v = (\dot{r}_{\max} - \dot{r}_{\min})/2 \quad \text{and} \quad a = (r_{\max} - r_{\min})/2,$$

respectively. Then the scaled dimensionless overall growth rate and amplitude are given by

$$v = (\dot{r}_{\max} - \dot{r}_{\min})/2W_i \quad \text{and} \quad a = (r_{\max} - r_{\min})/2R_0,$$

respectively.

Figure 5 shows the perturbation growth rate for all four classes. For all simulations the light fluid is air and the heavy fluid is SF_6. The results for the growth rate of the RM interface driven by an incident shock of Mach number $M = 1.2$, 10, 15, 40, and 100 are superimposed in Figure 5 and are shown in terms of scaled velocity and scaled time. The numerical simulations are conducted at a dimensionless grid spacing $\Delta\tilde{x} = \Delta\tilde{y} = \Delta x/R_0 = 0.0042$. At this

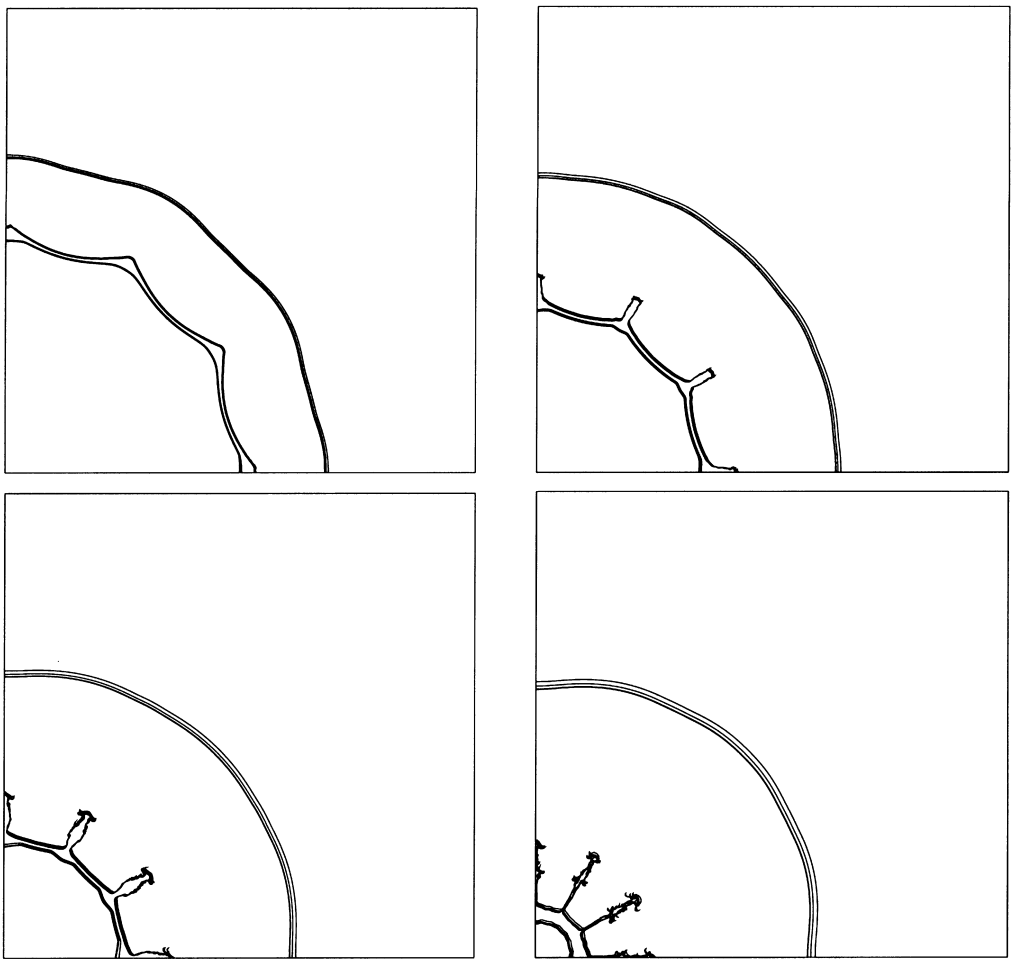

FIG. 7.—Evolution of the interfaces for class 2 (light-imploding-heavy), where Mach number 10, 15, 40, and 100 are superimposed at $\tilde{t} = 0.57$, 0.83, 1.0, 1.3 (*upper left*, *upper right*, *lower left*, *lower right*, respectively). The incident shock has bifurcated into a transmitted shock moving radially toward the origin and a reflected shock moving radially away from the origin. In terms of scaled time, the interfaces driven by different Mach number ($M \geq 10$) coincide and demonstrate a scaling law.

resolution, the numerical solution is no longer sensitive to the grid size. The initial (preshocked) dimensionless perturbation amplitude is $a/R_0 = 0.033$. In Figure 6 we show the corresponding scaled dimensionless perturbation amplitude as a function of the scaled time. Figures 5 and 6 showed that in the imploding (exploding) case, once the Mach number of the incident shock is larger than 15 (40), the scaled quantities are no longer sensitive to the incident shock strength. Therefore, RM unstable systems driven by strong shocks satisfy a nice scaling law. Let $v_{M_1}(t)$ be the growth rate of a RM unstable interface driven by a strong shock of Mach number M_1, where both v and t are dimensional quantities. Then the overall growth rate, $v_{M_2}(t)$, for a RM unstable interface driven by a strong shock of Mach number M_2 can be obtained from $v_{M_1}(t)$ by the scaling relation:

$$v_{M_2}(t) = \frac{M_1}{M_2} v_{M_1}\left(\frac{M_1}{M_2} t\right). \tag{1}$$

Similarly, the following scaling relation holds for the amplitudes:

$$a_{M_2}(t) = a_{M_1}\left(\frac{M_1}{M_2} t\right). \tag{2}$$

The results shown in Figures 5 and 6 are for the overall growth rate and amplitude of the RM unstable interface, which are global features. Will the shape of the interface also satisfy a scaling law? Our numerical simulations showed that it indeed does. In Figure 7, we superimpose the shapes of the Class 2 RM unstable interfaces driven by strong shocks of Mach number, $M = 10$, 15, 40, and 100. The inner and outer curves in Figure 7 are transmitted and reflected shock waves, respectively, and the curves between them are the material interfaces. The snapshots of the interfaces at four different times $\tilde{t} = 0.57$, 0.83, 1.0, and 1.3 are shown in Figure 7. It is obvious from Figure 7 that the following scaling law holds for the shape of the unstable interface:

$$\boldsymbol{R}_{M_2} = \boldsymbol{R}_{M_1}\left(\frac{M_1}{M_2} t\right). \tag{3}$$

Here $\boldsymbol{R}$ represents the location for the material interface, the shock waves or rarefaction wave. For comparison, the shape of the unstable material interface driven by a weak shock of Mach number 1.2 is shown in Figure 8 at the same scaled times. By comparing Figure 7 with Figure 8, we conclude that the shape of RM unstable interface driven by strong shocks and that driven by weak shocks are quite different. Therefore, the scaling law presented above does not hold for RM unstable interfaces driven by weak shocks.

The preshocked Atwood number between air and SF_6 is $A = 0.67213$. To further confirm the scaling laws given by equations (1)–(3), we present the results for the system in class 2 with preshocked Atwood number $A = 0.33333$ in

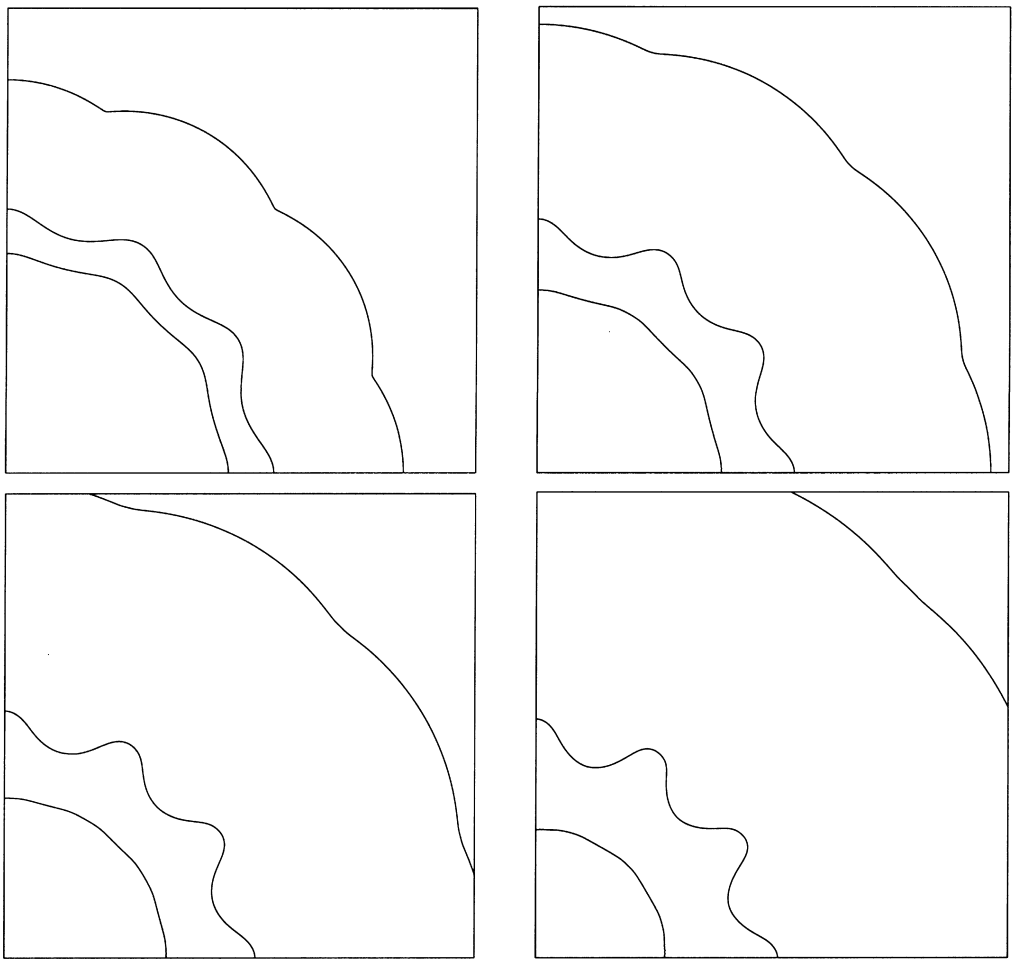

FIG. 8.—Evolution of the interface for class 2 (light-imploding-heavy) for Mach number 1.2. The frames shown in this figure are at the same dimensionless time as in Fig. 7. Note that the shape of the interface is quite different from those in Fig. 7. Therefore, the scaling law does not hold for weak shocks.

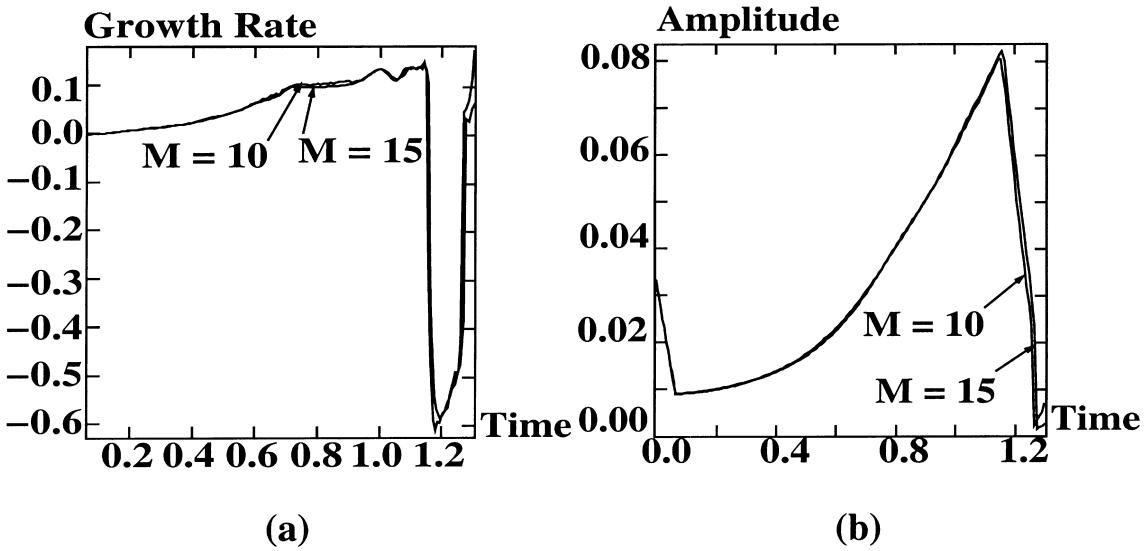

FIG. 9.—Comparison of the scaled growth rate and the scaled perturbation growth rate vs. scaled time for Mach numbers $M = 10$ and 15. Here the preshocked Atwood number is $A = 0.33333$.

Figure 9. The adiabatic exponents of the two fluids are the same as those of air and SF_6. Figure 9 shows that the scaling laws are indeed satisfied once the Mach number is larger than 10.

The scaling relations presented in this letter are important for studying the RM unstable systems driven by strong shocks (for a more detailed study, see Zhang & Graham 1998). It allows us to obtain the results for all strong shocks by conducting only one strong shock experiment or by performing one strong shock numerical simulation in that family. We have checked that this scaling relation also holds for RM unstable interfaces driven by strong shocks in planar geometry. We believe that this relation should hold in spherical geometry as well. We further speculate that this scaling law also holds for multimode RM unstable systems driven by strong shocks.

We would like to thank Dr. I-Liang Chern for helpful discussions and Dr. Bruce Remington for supporting this work. This work was supported in part by the US Department of Energy, contract DE-FG02-90ER25084 and National Science Foundation, contract NSF-DMS-9301200, City University of Hong Kong contract 7000776, and RGC contract 9040399.

REFERENCES

Chern, I.-L., Glimm, J., McBryan, O., Plohr, B., & Yaniv, S. 1986, J. Comput. Phys., 62, 83
Dimonte, G., Frerking, C. E., & Schneider, M. 1996, Phys. Plasmas, 3(2), 614
Meshkov, E. E. 1970, NASA Tech. Trans., F-13, 074
Richtmyer, R. D. 1960, Commun. Pure Appl. Math., 13, 297
Yang, Y., Zhang, Q., & Sharp, D. H. 1994, Phys. Fluids, 6(5), 1856
Zhang, Q., & Graham, M. J. 1998, Phys. Fluids, 10(4), 974